Authigenic, volcanogenic, and detrital influences on the Cenomanian–Turonian clay sedimentation in the Western Interior Basin: Implications for palaeoclimatic reconstructions

Guillaume Charbonnier, Delphine Desmares, Jérémie Bardin

Authigenic, volcanogenic, and detrital influences on the Cenomanian–Turonian clay sedimentation in the Western Interior Basin: Implications for palaeoclimatic reconstructions

Guillaume Charbonnier[1, 2*], Delphine Desmares[3], Jérémie Bardin[3].

1. Institute of Earth Sciences, Géopolis, University of Lausanne, CH-1015 Lausanne, Switzerland.

2. GEOPS, Univ Paris Sud, CNRS, Université Paris Saclay, Université Paris Sud, Bât 504, Orsay, F-91405, France.

3. CR2P - Centre de Recherche en Paléontologie - Paris - Sorbonne Université - MNHN - CNRS, Tour 46-56, 5ème, case 104, 4, place Jussieu, F-75005, Paris, France.

* Corresponding author.

E-mail address: guillaume.charbonnier@unil.ch (G. Charbonnier)

Telephone number: 00 41 (0) 21 692 43 10

Abstract

High-resolution changes in the mineralogical assemblages at Pueblo and Hot Springs of the Western Interior Basin (WIB, USA) were investigated for the late Cenomanian–early Turonian interval, including the Oceanic Anoxic Event 2 (OAE2). The aim of this study is to investigate the regional significance of clay mineral assemblages in the WIB by distinguishing authigenic, volcanogenic, and detrital influences. At Pueblo, the last few centimetres of the Hartland Shale and the Bridge Creek Limestone formations present an abrupt increase in R0 I-S content (up to 90% of the clay signal), which is coeval to an important incursion of subtropical Pacific seawater entered in the seaway from the Gulf of Mexico. We suggest that sea-level changes and volcanic activity expressed by bentonite horizons constitute the principal source of smectitic minerals found in the south central region of the basin. At equivalent stratigraphic interval in the Hot Springs section, situated 5° north of Pueblo (~600 km north), the smectitic sedimentation was mixed by local detrital input in kaolinite (from 6 to 45%). The great abundance of detrital kaolinite at the northern Hot Springs site is probably due to a very different clay provenance in that part of the seaway. It appears that two local supplies of kaolinite are recorded in the *S. gracile* ammonite zone (up to 45%) and in the latest Cenomanian–early Turonian interval (from 6 to 31 %). The particular geographic configuration of the Western Interior Basin (arrangement of landmasses and the seaway) in the tropical-subtropical environment initiate and maintain seasonally reversing movements of air mass, high evaporation flux, atmospheric heat transport, and precipitation. In this regards, we suggest that local kaolinite input reflect a more humid climate can be attributed to the local intensity of monsoonal-driven precipitation.

Keywords: Cenomanian–Turonian stage boundary, OAE2, volcanic activity, continental weathering, monsoonal circulation.

1. Introduction

The Cenomanian–Turonian boundary interval (~93.9 Ma, Meyers et al., 2012) recorded one of the most significant oceanic anoxic events of the Mesozoic. Oceanic Anoxic Event 2 (OAE2) (Schlanger and Jenkyns, 1976; Leckie et al., 2002; Jenkyns, 2010) was the time of exceptionally profound changes in the ocean-atmosphere system, which includes widespread organic-rich deposits referred to as the "Livello Bonarelli" in Italy or equivalent (e.g., Jenkyns, 2010) and a positive carbon isotope excursion recognized in sedimentary carbonate and organic matter fraction (e.g., Pratt, 1984; Schlanger et al., 1987; Paul et al., 1999; Kuypers et al., 2002; Tsikos et al., 2004; Jarvis et al., 2006; Grosheny et al., 2006; Sageman et al., 2006; Desmares et al., 2007; Joo and Sageman, 2014). The OAE2 interval is accompanied by exceptional warming of the ocean (Huber et al., 2002; O'Brien et al., 2017), briefly interrupted by a cooling event known as the "Plenus Cold Event" (Gale and Christensen, 1996; Forster et al., 2007; Jarvis et al., 2011). This time interval is also characterized by high levels of atmospheric CO_2 (Barclay et al., 2010), global sea level highstand (Haq, 2014), and turnover of marine biota (e.g., Eicher, 1969; Sigal, 1977; Elder, 1989; Leckie et al., 2002).

The nature of the clay fraction in marine sediments represents a useful proxy to investigate local palaeoenvironmental conditions because clay minerals are mainly inherited from continents depending to the geodynamic context, the type of weathered primary sediments, and climatic conditions. Particularly, during the late Cenomanian–Turonian period the distribution of clay minerals in the central part of Anglo-Paris Basin in the Poigny core is dominated by monotonous smectitic minerals (Deconinck et al., 2005). By contrast, in the north-east part of this basin, the clay fraction is characterized by local terrigenous input of illite and kaolinite derived from the Ardenne Massif source area (Debrabant et al., 1992). In addition to the local detrital sources, the occurrence of bentonite horizons in the late Turonian suggest the influence of volcanic activity (Deconinck et al., 2005). The complex distribution of clay mineralogy is controlled by the morphology and the

location of the studied sections in relation to the source areas (Deconinck et al., 2005). In strong contrast, clay mineralogy in the Agadir Basin (Central Morocco) suggests that humid conditions with large kaolinite input prevailed at the onset of OAE2, followed by dry seasonal conditions as indicated by high smectite contents (Daoudi et al., 2008; Gertsch et al., 2010a). Similar clay fraction trends were observed at the same palaeolatitude during the late Cenomanian–Turonian interval in the Sinay (Egypt; Gertsch et al., 2010b). By contrast, constant dry seasonal conditions are recorded in the Tarfaya Basin (southern Morocco; Gertsch et al., 2010a). These important geographical and stratigraphical variations in the clay fraction along the Africa margin have been attributed to variations in the Intertropical Convergence Zone and in the intensity of winds in tropical areas (Gertsch et al., 2010a, b).

The Jurassic–Cretaceous episodes of convergence of the Nevadan and Sevier Orogenies have led to the establishment of the Western Interior Basin (WIB), an elongated interior foreland marine basin (Kauffman, 1977; Hay et al., 1993). This basin was developed between the active American Cordilleran orogenic belt (Sevier Highlands) to the west (Jordan, 1981; Weimer, 1984) and the American stable craton to the east (Caldwell and Kauffman, 1993). This foreland basin is influenced by intense volcanic activity in the Cordillera, as suggested by the extensively deposited volcanic ash beds (bentonite) in marine sediments (Obradovich and Cobban, 1975; Kauffman, 1985; Elder, 1988; Cadrin et al., 1995). During the maximum Cretaceous transgression, the WIB was an area of hemipelagic sedimentation characterized by 200 to 500 m of depth, linking the Boreal Arctic realm to the proto Gulf of Mexico and Tethyan realm (Kauffman, 1977, 1984; Batt, 1987; Sageman and Arthur, 1994) (Fig. 1). A complex oceanographic regime into the basin was driven by the interplay between incursions of southern Tethyan and northern Boreal water in the North America seaway (Kauffman, 1984; Caldwell et al., 1993; Eicher and Diner, 1985; Arthur and Sageman, 1994; Elderback and Leckie, 2016) (Fig. 1). Major oceanographic re-organization during the transgression in the latest Cenomanian–Turonian interval promoted open marine oligotrophic conditions in the basin (Corbett and Watkins, 2013; Eldrett et al., 2014, 2017). Similar to the

105 African margin and Anglo-Paris Basin, the clay mineral distribution in the WIB was controlled by
106 the dynamic interactions among several factors, including the watermass dynamic in the basin, the
107 volcanogenic sources, and the multiple point source rivers delivering suspended load from both
108 sides of the seaway with very different clay provenances. The distinctive clay mineral assemblages
109 documented at three sections in the central and southwestern WIB attest that ocean circulation, in
110 addition to two disparate sources, in the seaway influenced the observed distribution of clay
111 minerals (Leckie et al., 1991, 1998).

112 The aim of this study is to investigate the regional significance of clay mineral assemblages
113 in the WIB by distinguishing between authigenic, volcanogenic, and detrital fractions. For this, we
114 document the evolution in the clay mineralogy in four different sections situated at different
115 latitudes of the western interior basin, which each includes the C–T boundary: Lohali Point
116 (Arizona), Pueblo (Colorado), Elm (Kansas), and Hot Springs (South Dakota).

117

118 **2. Geological setting**

119

120 Two sections sampled at high resolution were examined in the central axis of the seaway: (i)
121 the Pueblo section defined as the reference section of the WIB (GSSP for the base of Turonian,
122 Kennedy et al., 2005) and (ii) the Hot Springs section located 5° north of Pueblo (Fig. 1). Two
123 additional sections located in the western and the eastern margin of the basin have been studied in
124 order to characterize the potential spatial and temporal influences of differential settling, changes in
125 sources, and the potential variations in the intensity of continental weathering on clay minerals.

126 Precise correlations between these sections have been performed using the five major
127 centimetres-thick altered ash layers (bentonites) designated as A, B, C, D, and E (Elder, 1988;
128 Desmares et al., 2007) (Fig. S1 in supplementary material). Correlations are also supported by
129 macrofossil biostratigraphy (Elder, 1987a; Kennedy and Cobban, 1991) and the pattern of globally
130 recognized positive $\delta^{13}C$ excursion (Pratt, 1984; Pratt and Threlkeld, 1984; Caron et al., 2006;

Desmares et al., 2007). In addition, numerous cyclostratigraphic studies were conducted in different cores and sections in the central Western Interior Basin (Sageman et al., 2006; Meyers et al., 2012; Ma et al., 2014; Eldrett et al., 2015). The sampled interval includes the Cenomanian–Turonian boundary and coincides with OAE2 as expressed by the distinctive first and second positive $\delta^{13}C$ shift and C-plateau (Desmares et al., 2007) (Fig. S1).

2.1. The Pueblo section (Colorado)

Situated in the central axis of the WIB, the outcrop close to the locality of Pueblo, Colorado, USA, is a well-documented reference section. As this section is the GSSP for the base of the Turonian (Kennedy et al., 2005), the rich archive of previously acquired data (e.g., Cobban and Scott, 1972; Pratt, 1984; Leckie, 1985; Kennedy and Cobban, 1991; Morel, 1998; Caron et al., 2006; Desmares et al., 2007) provides stratigraphic constraints. The Hartland Shale is clay dominated whereas the Bridge Creek Limestone is composed of rhythmically bedded prominent limestones alternating with dark grey calcareous shales (Cobban and Scott, 1972; Pratt et al., 1985).

2.2. The Hot Springs section (South Dakota)

The outcrop is located close to Hot Springs, South Dakota, USA (Fig. 1). The sedimentary succession is composed of rhythmically bedded limestone beds alternating with dark grey marlstone/calcareous shales (Desmares, 2005). Bentonite marker beds A, B, C and D (Elder, 1987b; Desmares et al., 2007; Desmares et al., 2016) are recognised in this stratigraphic equivalent of the more southerly Bridge Creek Limestone in accordance with ammonite zonation (Elder, 1987b). Due to the poor outcrop exposures, the Hartland Shale was not sampled.

2.3. The western and eastern marginal sections (Lohali Point/Elm sections)

Two sections located at the same latitude as Pueblo, on the active western margin (Lohali Point, Arizona) and the eastern stable margin (Elm, Kansas) were investigated.

The outcrop of Lohali Point is situated on the eastern side of the Black Mesa basin in northeastern Arizona, which corresponded to a neritic environment along the southwestern side of the seaway (Kirkland, 1991). The lithology is dominated by shale in relation to the proximity of the tectonically active Sevier orogenic belt to the west (Kauffman, 1977; Elder, 1987b; Kirkland, 1991). The sedimentary succession is well dated by ammonites (e.g., Elder, 1987b; Kirkland, 1991). The Elm section (Kansas), located on the south side of the Wilson Lake, close to Bunker Hill, is dominated by limestone interbedded with dark calcareous shales (Desmares et al., 2007). This outcrop is located in a neritic environment, on the stable eastern craton to the East and to the northwest of the Ouachita Mountains (Fig. 1).

3. Methods

3.1. Mineralogical analyses

The surface of each sample was cleaned and fresh unweathered samples were collected for analyses. A total of 70 samples were investigated for clay mineralogy analysis using X-ray Diffraction (XRD) method. The samples were prepared at the University of Paris Sud in the GEOPS Laboratory ("GEOsciences Paris Sud"). They were treated successively with diluted acetic acid (CH_3COOH) and hydrogen peroxide (H_2O_2) to remove carbonates and organic matter. Successive washing in distilled water allowed clay deflocculation. The □2 μm clay fraction was then separated from the bulk samples by the settling method according to Stoke's law. The clay fraction was pipetted and deposited on a glass plate, then dried at room temperature. Three X-ray diagrams were measured using a PANalytical Diffractometer: one after air drying, one after ethylene glycol

183 solvation for 24 h and one after heating at 490°C for 2 h. Clay minerals were identified based on the
184 position of the (001) series of basal reflections on the curve with the MacDiff software (Petschick,
185 2000) using the main X-ray diffraction peaks of each mineral (mixed-layers illite-smectite: 12-17Å;
186 illite: 10Å and kaolinite/chlorite: 7Å). Relative proportions of kaolinite and chlorite were
187 determined using the 3.57 and 3.54Å peaks respectively. Measurements of illite layers in mixed-
188 layered (I-S) were performed following the procedure of Moore and Reynolds (1997). Analytical
189 uncertainties are estimated to be 5%.
190
191 3.2. Degree of correlation between clay mineral species and paleoenvironment
192
193 To emphasize the relationships between the different clay mineral species and
194 environmental triggers, we search for correlations between the different types of clay and both the
195 $\delta^{18}O_{carb}$ and the percentage of sinistral forms of *Muricohedbergella delrioensis* that is significantly
196 correlated with temperature (Desmares et al., 2016). For each couple of variables used for
197 correlation tests, we only keep points that were measured for the two considered variables. This
198 means that the removal of samples is done for a given pair of variables independently from another
199 pair. This allows conserving the maximum amount of information for each pair of variables subject
200 to correlation test (Fig. S2 in supplementary material). Basically, it simply corresponds to remove
201 the observations with missing values after the selection of the variables constituting a pair. To
202 assess from short to long-term correlations, we compute non-overlapping moving averages with
203 different window sizes (from 1 to 5). All the variables are time series (both the raw variables and
204 the non-overlapping moving averages) and, since Yule (1926), we know that significant correlations
205 between time series may be spurious. Indeed, autocorrelation of time series make successive values
206 close to each other. As a consequence, two time series showing significant autocorrelations are very
207 likely correlated because of chance alone (Box, 1994). To avoid this bias, we have computed the
208 autocorrelation functions of all variables with the function *acf* from the '*stats*' package (R Core

Team, 2018). If at least one of the two variables shows a significant autocorrelation at lag = 1, we compute and use differences ($dX = X_t - X_{t-1}$). Once, no autocorrelation remains in the variables (differenced or not), we perform correlations with Pearson correlation coefficient because the linearity of relationships between variables has been eyed-checked. We use p-values as a measure of the robustness of the results.

4. Results

During the Cenomanian–Turonian boundary interval, clay minerals identified in the fraction <2 μm include irregular illite-smectite mixed layers (R0 I-S), kaolinite, illite, and chlorite (Figs. 2, 3, 4).

4.1. The Pueblo section (Colorado)

Clay mineral assemblages (fraction <2 μm) of the Pueblo section are composed of R0 I-S mixed layers, kaolinite, illite, and chlorite. Given the distribution of these minerals the section can be divided in two intervals that correspond to the two lithologic members.

The first interval (uppermost part of the Hartland Shale, below the base of Bridge Creek Limestone Bed 63; Cobban and Scott, 1972) is marked by significant changes in the clay mineralogy (Fig. 2). Starting with values around 2%, the kaolinite contents increases significantly up to 15%, whereas the R0 I-S mixed layers decreases from 69 to 59%. Illite and chlorite contents show relatively stable values with an average of 21% and 5%, respectively. Thereafter, a drop in kaolinite and illite contents is recorded. The irregular R0 I-S rises toward a maximum of 90%.

The second interval covers the lower Bridge Creek Limestone (from the base of the limestone marker Bed 63 up to the bentonite D) is largely dominated by R0 I-S (>80%, with an average proportion of 92%) with rather low values of kaolinite and chlorite never exceeding 3%

(Fig. 2). The illite-smectite irregular mixed-layers contain more than 80% of smectite layers.

4.2. The Hot Springs section (South Dakota)

In the residue of the <2 μm fraction, kaolinite and R0 I-S (mineral containing 60% of smectite layers) dominate the assemblages, with an average of 42 and 27%, respectively (Fig. 2). Given the distribution of these two clay minerals the section can be divided into four intervals (Fig. 2). The first interval (within the *Sciponoceras gracile* ammonite zone) is characterized by significant rise in R0 I-S contents (from 1 to 39%). An inverse trend is recorded for the illite (from 51 to 18%). The kaolinite content curve shows rather high and stable values (with an average of 36%). Chlorite content displays relatively high values (>10%) at the base of the section and relatively low and constant values (<5%) for the upper part (Fig. 3). The second interval comprises the uppermost part of the *S. gracile* ammonite zone up to the bentonite marker bed B in mid-*Neocardioceras juddii* ammonite zone (Fig. 3). The kaolinite and illite proportions gradually decreases (from 37 to 7%, and from 29 to 1% respectively), whereas the illite-smectite mixed layer drastically increases to 92%. In the *N. juddii* ammonite zone, kaolinite contents display a long-term increasing trend with a maximum value of 33% near the Cenomanian–Turonian boundary. This trend is coeval with illite proportions, and opposite to the R0 I-S content reaching a minimum value of 46% (Fig. 3). Finally, in the last interval between the bentonite marker beds C and D the assemblages show a gradual change from 17 to 31% for kaolinite, and 19 to 35% for illite. The R0 I-S proportions drop to values between 32 and 33% (Fig. 3).

4.3. The Lohali Point (Arizona) and Elm (Kansas) sections

The clay mineralogy of the Lohali Point section is largely dominated by R0 I-S mineral, with an average proportion of 93% (Fig. 4). The illite/smectite irregular mixed-layers contain more

than 80% of smectite. The kaolinite, illite, and chlorite contents show very low values never exceeding 5% (Fig. 4).

As observed at Lohali Point, irregular illite-smectite mixed layers largely dominate the clay mineralogical assemblage in the Elm section with values ranging between 90 and 96% (Fig. 4). The illite/smectite irregular mixed-layers contain more than 80% of smectite. Kaolinite, illite, and chlorite contents never exceed 4% of the clay mineral assemblage (Fig. 4).

5. Discussion

The mineralogical composition of whole rock in marine sediments is mainly the product of multiple processes that include (i) diagenetic overprint, (ii) the differential settling of clay minerals, (iii) the structural evolution of the adjacent landmasses and associated sea-level changes, (iii) the alteration of volcanic rocks, (iv) the composition of weathered primary rocks, and (v) the weathering conditions, which varies with climate (Singer, 1984; Chamley, 1989; Deconinck and Chamley, 1995; Thiry, 2000; Adatte et al., 2002; Deconinck et al., 2005; Charbonnier et al., 2016). The resulting different clay mineral assemblages observed in the WIB sections may be the result of one or more of these processes (Fig. 2).

5.1. Burial diagenetic overprint in the WIB

In Mesozoic Tethyan sequences, the original mineralogical signal may have been significantly modified by diagenetic overprint (Chamley and Deconinck, 1985; Chamley, 1989; Thiry, 2000). Burial diagenesis, depending of the tectonic history, is responsible for clay mineral transformation (Deconinck, 1987; Chamley, 1989; Thiry, 2000). Smectite is very sensitive to high temperature linked to burial history (Chamley, 1989). Progressive illitization in the marly interbeds and chloritization in the calcareous beds of original smectite is evidenced by the gradually decrease

of smectite with depth (Deconinck and Debrabant, 1985; Lanson and Meunier, 1995). Diagenetic transformation is marked by the appearance of regularly interstratified illite-smectite minerals.

The presence of irregular I-S R0 minerals rich in smectite layers (>50% of smectite layers) indicates that sedimentary series in the WIB were not subjected to strong diagenetic burial. The clay mineralogical assemblage is rather diversified and the presence of significant variations (>5%) in the clay minerals, such as kaolinite, suggests only a moderate impact of the burial diagenesis. Finally, this is confirmed by the T_{max} values at Lohali Point and Pueblo, which never exceed 435°C (Leckie et al., 1998; Dellisanti et al., 2010). Rock eval data suggest moderate burial depth below the oil-generating window (< 2500 m), which is compatible with the presence of R0 I-S (Leckie et al., 1998; Dellisanti et al., 2010). Consequently, in the WIB chloritization and illitization of smectite seems of minor importance in the clay mineral assemblages.

5.2. Differential settling processes

The differential settling of clay minerals is the result of the physical segregation of minerals during transport of particles in relationship to their different size and flocculation (Chamley, 1989). The distribution of clay minerals in sediments can be largely impacted by this process. Kaolinite and illite are dense and coarse minerals that settle preferentially closer to the coast, near to the shore in platform environments. Conversely, smectite is a fine-grained mineral that settles much more slowly in deeper waters in more offshore settings. As a consequence, the relative proportions of illite/kaolinite compared to smectite can be a proxy of distance to the shoreline and therefore sensitive to advance (regression) and retreat (transgression) of the shoreline (sea) (Chamley, 1989; Duchamp-Alphonse et al., 2011).

In the Western Interior Basin, a West-East transect along a proximal area to a more distal area allows to estimate the differential settling (Fig. 2). Curiously, the high values (> 80%) of smectite-rich I-S mixed layers are recorded in the marine sediments of the Lohali Point and Elm

sections located on the more proximal sides of the seaway. Similarly, the relative high values of kaolinite and illite contents are recorded in the section of Hot Springs and to a lesser extent in the section of Pueblo situated in the central axis of the basin. Thus, it seems that the differential settling processes not play a major role in the clay assemblage distribution in the WIB.

5.3. Significance of authigenic kaolinite fraction

Scanning electron microscope (SEM) examinations of the internal content of foraminiferal tests from several stratigraphic levels of the Hot Springs sections were undertaken to provide more information on potential authigenic phases (Fig. 5). In sample HS9 (*S. gracile* ammonite zone, kaolinite content: 32%), SEM examinations reveal that a large authigenic kaolinite phase occurs in foraminiferal tests (Fig. 5), but no authigenic kaolinite phase was found in the other samples (HS3, HS5, HS26, and HS62) despite high kaolinite content in some levels.

Occurrences of authigenic kaolinite within foraminiferal tests have been also identified in other Upper Cretaceous formations of the same sedimentary basin (Pollastro, 1981). These authors suggest that after burial, volcanic detritus may have formed colloidal aluminous gel and moved in large pore space such as formaniferal tests. Bacterial decomposition of organic matter under low pH conditions is favourable for crystallisation of kaolinite (Pollastro, 1981). Similarly, at Poigny and Sainte Colombe in the Anglo-Paris Basin authigenic kaolinite occurs in bentonite layers (Deconinck et al., 2005). These unusual authigenic kaolinite-rich deposits have been probably formed shortly after burial in reducing environments (Deconinck et al., 2005). Curious spikes in kaolinite (A to E, up to 35%) have been also found in samples from Pueblo section at the top of the *S. gracile* Zone and at the base of the *N. juddii* Zone (Leckie et al., 1991, 1998). This relatively rich kaolinite interval recorded across the seaway (Leckie et al., 1998) can be correlated to relative sea level fall or progradation event at the base of the *N. juddii* in western Iowa (Elderbak et al., 2014). These spikes may be explained by differential settling of clay minerals, which are sensitive to advance of

339 the shoreline. One another possibility is that this unique level at Hot Springs may be explained by
340 reworking of volcanic ash in oxygen depleted environments.
341
342 5.4. Sea-level changes versus volcanogenic origin of the smectitic minerals
343
344 Smectitic minerals (R0 I-S mixed layers) are the major components (>50%) of the clay
345 fraction of the Cenomanian–Turonian sediments along the WIB sections (Figs. 2-4). High
346 concentrations of smectite in marine sediments derive mainly from seasonally contrasted semi-arid
347 conditions, volcanogenic clays derived from submarine weathering of volcanic glass, or sea-level
348 changes (Chamley, 1989; Deconinck and Chamley, 1995; Adatte et al., 2002).
349 The western margin of the Western Interior Basin is composed of an important active
350 explosive volcanic system (i.e., an Andean type magmatic belt), which extended continuously along
351 the western margin of the seaway from Alaska to Mexico (e.g., Kauffman and Caldwell, 1993).
352 Numerous centimetres thick volcanic ash beds interrupting marine succession are the expression of
353 major volcanic eruptions. Dozens and dozens of minor eruptions create millimetres thick bentonites
354 and represent a background source of volcanic minerals in the sediments. More than 1300 volcanic
355 ash beds have been described through the 38 Myr record of late Albian-Maastrichtian interval
356 (Obradovich and Cobban, 1975; Kauffman and Caldwell, 1993; Cadrin et al., 1995). In such
357 context, a significant proportion of I-S R0 in the seaway is volcanogenic and non-terrigenous.
358 A major change in clay mineralogical assemblage is observed at Pueblo, between the
359 Hartland Shale and the Bridge Creek Limestone members of the Greenhorn Formation, with
360 significant rise in R0 I-S contents up to 90% (Fig. 6). A similar increase in smectite is also
361 documented by Leckie et al., (1991, 1998) at Lohali Point. In the Bridge Creek Limestone and
362 equivalent strata, similar high R0 I-S contents (>80%) are recorded at Lohali Point, Pueblo, and
363 Elm in the bentonite A-C interval (Fig. 4). The increasing abundance of smectite is consistent with a
364 decrease in kaolinite observed at Lohali Point (Leckie et al., 1998) and Pueblo (This Study). This

time interval is recognized as the time of eustatic rise to culminate in the highest sea levels of the Cretaceous period in the early Turonian (late in the *Watinoceras* or early *Mammites* Zones) (Elder and Kirkland, 1993; Sageman, 1996; Arthur and Sageman, 2005). In the Western Interior Basin, during the Cenomanian-Turonian eustatic rise (*S. gracile* ammonite zone) an important incursion of subtropical Pacific seawater entered in the seaway from the Gulf of Mexico (Fisher et al., 1994; Leckie et al., 1998; Corbett and Watkins, 2013; Elderbak and Leckie, 2016). This is supported by invasion of warm water molluscs, foraminifera, and calcareous nannofossils (Caldwell et al., 1993; Fisher et al., 1994; Corbett and Watkins, 2013), by positive excursion in ε_{Nd} documented in marine sediments from Atlantic Sites (MacLeod et al., 2008; Martin et al., 2012), and by several Hg and Hg/TOC ratios enrichments in southern Western Interior Seaway and Demerara Rise sections (Scaife et al., 2017). This incursion of warm oxygenated water masses into seaway corresponds exactly to major change in clay mineralogical assemblage (Leckie et al., 1998; This Study). Variations in the kaolinite/smectite ratio may reflect sea-level changes (Adatte et al., 2002). During sea-level highstand, deposition of smectite can be attributed to sedimentary segregation of particles in more offshore setting. In addition, increased carbonate contents observed in the Bridge Creek Limestone in strong contrast to the Hartland Shales formation attests a more distant detrital source and thus deeper water conditions. This interpretation is supported by previous study, which suggests that clay mineralogy assemblages are likely influenced by circulation in the seaway (Leckie et al., 1998). Consequently, sea-level changes and volcanic activity constitute the principal source of smectite found in the WIB sediments.

5.5. Detrital kaolinite fraction at Hot Springs: implications for local palaeoclimatic reconstruction?

In strong contrast, in the same stratigraphic interval (bentonite A-C), the smectitic-rich sediments (>80%) interval recorded at Pueblo, Lohali Point or Elm are not observed in the Hot Springs section situated 5° north of Pueblo. The clay mineral assemblages are also dominated by I-

S mixed layers (from 1 to 92%), but associated with a significant proportion of kaolinite (from 6 to 45%) (Fig. 3). Particularly, the evolution of kaolinite abundances can be divided into three parts. (1) In the *S. gracile* ammonite zone, the kaolinite contents are high (up to 45%). (2) It is followed by a decreasing trend (from 45 to 6 %) in the *S. gracile-N. juddii* ammonite zones in the latest Cenomanian. (3) Finally, a long-term increasing trend from 6 to 31 % is observed from the latest Cenomanian to early Turonian (Fig. 6). The great abundance of detrital kaolinite (from 6 to 45%) at the northern Hot Springs site is probably due to a very different clay provenance in that part of the seaway. The clays accumulated are derived from the multiple rivers draining into the seaway probably from the eastern craton and Ouachita Mountain area (Leckie et al., 1991, 1998). There is probably a volcanogenic signal (smectite supply) that overprints the detrital influences (kaolinite supply).

One possible explanation is that the supply of kaolinite from rivers draining into the seaway reflects the high physical erosion of older rocks rich in kaolinite. Indeed, there could be a long time gap between clay mineral development in soils and their final deposition in the basin (Thiry, 2000; Dera et al., 2009). Strong erosion of Devonian or Carboniferous sedimentary rocks, considered to have significant amounts of kaolinite, could be a potential source area of kaolinite in the basin (Hillier et al., 2006; Shaw, 2006). In such cases, this process may seriously alter the palaeoclimatic signal of kaolinite in sedimentary records (Thiry, 2000).

Another possibility is that the formation of kaolinite in alterations was contemporaneous with sedimentation and was mainly inherited from landmasses during highly hydrolytic weathering conditions (Chamley, 1989; Dera et al., 2009). The latest Cenomanian-earliest Turonian interval represents one of the warmest periods of the Phanerozoic eon, with high atmospheric pCO_2 levels and the development of intensified greenhouse conditions (Huber et al., 2002; O'Brien et al., 2017). During this interval, the Western Interior Basin is situated in the tropical-subtropical setting, in the northern mid-latitude warm humid belt (am End, 1991; Chumakov et al., 1995; Skelton et al., 2003). Kaolinite deposits in recent sediments near tropical region in wet climate zones are mainly

linked to climatic conditions. Model simulations of Campanian indicate that a strong monsoonal existed due to the special configuration of the seaway (Fricke et al., 2010). Climate model simulations suggest also that monsoonal atmospheric circulation occurred earlier in Cretaceous (DeConto et al., 1999; Poulsen et al., 1999, 2007). Moreover, tropical storms were probably initiated in the central WIB toward the eastern margin (White et al., 2001). Other model results show that landmass distribution in the basin affect land sea air circulation, wind patterns, and precipitations (Glancy et al., 1993; Poulsen, 1999). Estimates of Cenomanian precipitation rates based upon the mass-balance modeling of the WIB is to ~3600 mm/year at ~45°N paleolatitude (Hot Springs section), which is significantly higher than today (3.6× present values) (Ufnar et al., 2008). Furthermore, these authors suggest that the heat transferred to the atmosphere via latent heat of condensation was approximately 10.6 higher than the present at 50°N. In this specific case we suggest that the existence of intense evaporation rates, winds patterns and seasonal rainfall is consistent with tropical wet climatic zone and the abundance of kaolinite in the Hot Springs sediments. Consequently, the two large increases in kaolinite in the *S. gracile* ammonite zone (values up to 45%) and in the latest Cenomanian–early Turonian interval (from 6 to 31%) indicates a more humid climate that can be linked to a local acceleration of hydrologic cycle. Leckie et al. (1991) suggest also that regional climatic warming and increased weathering accompanying the northward advance of warm normal marine waters during the latest Cenomanian transgression. In this regards, the local intensification of monsoonal-driven precipitations due to the special configuration of the seaway contribute to the successive humid episodes during the late Cenomanian–early Turonian interval.

5.6. Degree of correlation between kaolinite and other environmental variables: implications for oxygen isotope significance

Significant kaolinite enrichments at Hot Springs is probably related to climate change with

high precipitation and runoff in tropical zone. The proportion of left-coiled *M. delrioensis* in the planktonic foraminiferal assemblages represents a new proxy for constraining SST (°C) variations (Desmares et al., 2016). At the opposite, in the WIB, the significance of the $\delta^{18}O_{carb}$ signal remains largely debated. Some authors attest that the low negative $\delta^{18}O_{carb}$ values at Pueblo have been diagenetically altered (Pratt et al., 1993). Keller et al. (2004) suggest that the fluctuations in the $\delta^{18}O_{carb}$ variations are the effects of mixing between marine incursion and fresh water influx. By contrast, statistically highly significant correlation between $\delta^{18}O_{carb}$ and sinistral proportions indicate that these two data sets have been influenced by the same environmental effects (Desmares et al., 2016).

Short and long-term relationships are investigated between these environmental variables (Table 1) (Fig. S2 in supplementary material). For the high frequency variations between kaolinite and the $\delta^{18}O_{carb}$ and the abundance of sinistral *M. delrioensis*, the raw correlation is less than 0.25 (r=0.25-0.05 and r=-0.23 and -0.13, respectively) and p-values are higher than 0.4, which indicate that the correlation between these environmental variables is not significant (Table 1). The weak correlation observed in high frequency variations may be explained by the delay between the short response of proxies to seawater temperature changes and the timing of clay mineral formation in soils and their erosion, transport, and subsequent deposition in marine sediments due to the intensity of continental weathering (Thiry, 2000). In contrast, for the long-term frequency variations the raw correlation is greater than 0.9 (0.91 and 0.96, respectively) and the p values are less than 0.05 (0.03 and 0.01 respectively), which indicate the strong correlation between these data sets (Table 1). These results show the robustness of the long-term trends in the mineralogical and geochemical data sets for palaeoclimatic interpretation. The concordant evolution between kaolinite variations slightly affected by diagenetic influences and the environmental variables ($\delta^{18}O_{carb}$ and % sinistral form of *M. delrioensis*) support the interpretation of the $\delta^{18}O_{carb}$ variations in terms of temperature signal (Desmares et al., 2016) rather than the effects of mixing between marine incursion and fresh water influx. These two signals suggest that two cooling intervals in the upper part of the Hartland

Shale (S1a) and in the lower part of the Bridge Creek Limestone (S1b) may have occurred in the WIB (Desmares et al., 2016) (Fig. 6). The S1b cooling event, interpreted as the expression of the Plenus Cold Event in the WIB (Desmares et al., 2016), has also been recognized in several Atlantic and European basins by TEX_{86} data (Forster et al., 2007; Sinninghe Damsté et al., 2010; van Helmond et al., 2014), temporary influx of Boreal fauna (Gale and Christensen, 1996), and positive $\delta^{18}O$ excursion (Paul et al., 1999; Huber et al., 2002; Jenkyns et al., 2017; Kuhnt et al., 2017). The contemporaneity of this event in various basins at different latitudes suggest the existence of climatic cooling at the global scale, which is mainly explained by massive burial of organic carbon in sediments (Jarvis et al., 2011). In the WIB this global event was superimposed on the kaolinite supply expressed at the local scale due to the combination of the special configuration of seaway (sea-land distribution) and the tropical latitudinal position (northern mid-latitude humid belt).

6. Conclusion

New mineralogical data from the Pueblo, Hot Springs, Elm and Lohali Point sections were documented for the Western Interior Basin during the Cenomanian–Turonian boundary time interval, which includes the OAE2. It appears that the mineralogical trends reflect a primary signal. During the Cenomanian-Turonian eustatic rise the incursion of warm oxygenated water masses into seaway corresponds exactly to a major change in clay mineralogical assemblage with a significant rise in R0 I-S up to 90% and a decrease in kaolinite contents at Pueblo. In this interval the mineralogical distribution in the south-central region of the basin is mainly influenced by sea-level fluctuations. In the WIB the large distribution of bentonite horizons and volcanic ash layers in sediments indicates very important volcanic activity. In such context a significant proportion of I-S R0 (smectites) is volcanogenic and non-terrigenous. Consequently, we suggest that sea-level changes and volcanic activity constitute the two principal source of smectitic minerals found in this area.

By contrast, in the same stratigraphic interval major kaolinite enrichments occur at Hot Springs, situated 5° north of Pueblo, in the *S. gracile* ammonite zone (up to 45%) and in the latest Cenomanian-Turonian interval (from 6 to 31%). The great abundance of detrital kaolinite at the northern site is probably due to a very different clay provenance in that part of the seaway. The special geographic configuration of the Western Interior Basin (arrangement of continent and the seaway) in the tropical-subtropical environment initiate and maintain seasonally reversing movements of air mass, high evaporation flux, atmospheric heat transport and precipitation. Significant kaolinite enrichment at Hot Springs is probably related to local humid conditions developed during monsoonal air mass movements. The concordant evolution between kaolinite variations slightly affected by diagenetic influences and the environmental variables ($\delta^{18}O_{carb}$ and % sinistral form of *M. delrioensis*) support the interpretation of the $\delta^{18}O_{carb}$ variations, measured at both Pueblo and Hot Springs, in terms of temperature signal. In the WIB, the global expression of the Plenus Cold Event is surimposed to the local input of kaolinite due to the special configuration of seaway in the tropical setting.

Acknowledgments

We are grateful to Bernard Beaudoin (Mines-ParisTech) and Danièle Grosheny (University of Lorraine) for their advice, help, and collecting the samples. We would like to thank the Navajo tribes for permission to conduct field work on their tribal lands. We would also like to acknowledge the editorial assistance of Eduardo Koutsoukos. Mark Leckie and an anonymous reviewer are acknowledged for their helpful and very constructive reviews.

References

Adatte, T., Keller, G., Stinnesbeck, W., 2002. Late Cretaceous to Early Palaeocene climate and sea-

level fluctuations: the Tunisian record. Palaeogeography, Palaeoclimatology, Palaeoecology 178, 165–196.

am Ende, B.A., 1991, Depositional environments, palynology, and age of the Dakota Formation, *in* Nations, J.D., and Eaton, J.G., eds., Stratigraphy, depositional environments, and sedimentary tectonics of the western margin, Cretaceous Western Interior Seaway: Geological Society of America Special Paper 260, 65–84.

Arthur, M.A., Sageman, B.B., 1994. Marine black shales: depositional mechanisms and environments of ancient deposits: Annual Review of Earth and Planetary Sciences 22, 499-551.

Arthur, M.A., Sageman, B.B., 2005. Sea level control on source rock development: perspectives from the Holocene Black Sea, the mid-CretaceousWestern Interior Basin of North America, and the Late Devonian Appalachian Basin. In: Harris, N.B. (Ed.), The Deposition of Organic Carbon-Rich Sediments: Models, Mechanisms and Consequences. Society for Sedimentary Geology, Tulsa, pp. 35-59.

Barclay, R.S., McElwain, J.C., Sageman, B.B., 2010. Carbon sequestration activated by a volcanic CO_2 pulse during Ocean Anoxic Event 2. Nature geoscience 3, 205–208.

Box, G., 1994. Time series analysis: forecasting and control. Englewood Cliffs, NJ: Prentice Hall.

Batt, R., 1987. Pelagic biofacies of the Western Interior Greenhorn Sea (Cretaceous): evidence from ammonites and planktonic foraminifera. Unpublished PhD Dissertation, University of Colorado, 417pp.

Cadrin, A.A.J., Kyser, T.K., Caldwell, W.G.E., Longstaffe, F.J., 1995. Isotopic and chemcial compositions of bentonites as paleoenvironmental indicators of the Cretaceous Western Interior Seaway. Palaeogeography, Palaeoclimatology, Palaeoecology 119, 301-320.

Caron, M., Dall'Agnolo, S., Accarie, H., Barrera, E., Kauffman, E.G., Amédro, F., Robaszynski, F., 2006. High-resolution stratigraphy of the Cenomanian/Turonian boundary interval at Pueblo (USA) and Wadi Bahloul (Tunisia): stable isotope and bio-events correlation. Geobios 39,

171–200.

Caldwell, W.G.E., Kauffman, E.G., 1993. Evolution of the Western Interior Basin. Geological Association of Canada Special Paper 39, 680 pp.

Caldwell, W. G. E., Diner, R., Eicher, D. L., Fowler, S. P., North, B. R., Stelk, C. R., von Holdt, W. L., 1993. Foraminiferal biostratigra- phy of Cretaceous marine cyclothems, in: Evolution of the West- ern Interior basin: Geological Association of Canada Special Paper, edited by: Caldwell, W. G. E. and Kauffman, E. G., 39, 477– 520.

Chamley, H., 1989. Clay Sedimentology. Springer- Verlag, Berlin. 623 pp.

Chamley, H., Deconinck, J.F., 1985. Expression de l'évolution géodynamique des domaines nord-atlantique et subalpin au Mésozoïque supérieur, d'après les successions sédimentaires argileuses. C.R. Acad. Sci. (II) 300/20, 1007-1012.

Charbonnier, G., Duchamp-Alphonse, S., Adatte, T., Föllmi, K.B., Spangenberg, J.E., Gardin, S., Galbrun, B., Colin, C., 2016. Eccentricity paced monsoon-like system along the northwestern Tethyan margin during the Valanginian (Early Cretaceous): new insights from detrital and nutrient influxes into the Vocontian basin (SE France). Palaeogeography, Palaeoclimatology, Palaeoecology 443, 145-155.

Chumakov, N.M., Zharkov, M.A., Herman, A.B., Doludenko, M.P., Kalandadze, N.N., Lebedev, E.L., Rautian, A.S., 1995. Climatic zones in the middle of the Cretaceous period. Stratigr. Geol. Correl. 3, 3–14.

Cobban, W. A. and Scott, G. R., 1972, Stratigraphy and ammonite fauna of the Graneros Shale and Greenhorn Limestone near Pueblo, Colorado: U.S. Geological Survey Professional Paper, 645, 108 p.

Corbett, M.J., Watkins, D.K., 2013. Calcareous nannofossils paleoecology of the mid-Cretaceous Western Interior Seaway and evidence of oligotrophic surface waters during OAE2. Palaeogeography, Palaeoclimatology, Palaeoecology 392, 510–523.

Daoudi, L., Rocha, F., Ouajhain, B., Dinis, J.L., Chafiki, D., Callapez, P., 2008.

573 Palaeoenvironmental significance of clay minerals in Upper Cenomanian-Turonian sediments
574 of the Western High Atlas Basin (Morocco). Clay minerals 43, 615-630.
575 Debrabant, P., Chamley, H., Deconinck, J.F., Récourt, P., Trouiller, A., 1992. Clay sedimentology,
576 mineralogy and chemistry of Mesozoic sediments drilled in the northern Paris Basin.
577 Scientific Drilling 3, 138-152.
578 Deconinck, J.F., 1987. Identification de l'origine détritique ou diagénétique des assemblages
579 argileux: le cas des alternances marne-calcaire du Crétacé inférieur subalpin. Bull. Soc. Géol.
580 Fr. 8, 139–145.
581 Deconinck, J.F., Debrabant, P., 1985. Diagenèse des argiles dans le domaine subalpin: rôles
582 respectifs de la lithologie, de l'enfouissement et de la surcharge tectonique. Revue de
583 Géologie Dynamique et de Géographie Physique 26, 321–330.
584 Deconinck, J.F., Chamley, H., 1995. Diversity of smectite origins in Late Cretaceous sediments:
585 example of chalks from northern France. Clay Minerals 30, 365-379.
586 Deconinck, J.F., Amédro, F., Baudin, F., Godet, A., Pellenard, P., Robaszynski, F., Zimmerlin, I.,
587 2005. Late Cretaceous palaeoenvironments expressed by the clay mineralogy of Cenomanian-
588 Campanian chalks from the east of the Paris Basin. Cretaceous Research 26, 171-179.
589 DeConto, R.M., Brady, E., Bergengren, J.C., Thompson, S.L., Pollard, D., Hay, W.W., 1999. Late
590 Cretaceous climate, vegetation, and ocean interactions. In: Huber, B., MacLeod, K.G., Wing,
591 S.L. (Eds.), Warm Climates in Earth History. Cambridge University Press, pp. 275–297.
592 Dellisanti, F., Pini, G.A., Baudin, F., 2010. Use of Tmax as a thermal maturity indicator in orogenic
593 successions and comparison with clay mineral evolution. Clay minerals 45, 115-130.
594 Dera, G., Pellenard, P., Neige, P., Deconinck, J.F., Pucéat, E., Dommergues, J.L., 2009.
595 Distribution of clay minerals in Early Jurassic Peritethyan seas: Palaeoclimatic significance
596 inferred from multiproxy comparisons. Palaeogeography, Palaeoclimatology, Palaeoecology
597 271, 39-51.
598 Desmares, D., 2005. Enregistrement à haute resolution des modifications environnementales

599 inscrites dans un cadre tephrochronologique: le basin du Western Interior au passage
600 Cénomanien-Turonien. Unpublished PhD Dissertation, University of Strasbourg 1, 440pp.
601 Desmares, D., Grosheny, D., Beaudoin, B., Gardin, S., Gauthier-Lafaye, F., 2007. High resolution
602 stratigrapic record constrained by volcanic ash beds at the Cenomanian-Turonian boundary in
603 the Western Interior Basin, USA. Creatceous Research 28, 561–582.
604 Desmares, D., Crognier, N., Bardin, J., Testé, M., Beaudoin, B., Grosheny, D., 2016. A new proxy
605 for Cretaceous paleoceanographic and paleoclimatic reconstructions: Coiling direction
606 changes in the planktonic foraminifera Muricohedbergella delrioensis. Palaeogeography,
607 Palaeoclimatology, Palaeoecology 445, 8-17.
608 Duchamp-Alphonse, S., Fiet, N., Adatte, T., Pagel, M., 2011. Climate and sea-level variations along
609 the northwestern Tethyan margin during the Valanginian C-isotope excursion: mineralogical
610 evidence from the Vocontian Basin (SE France). Palaeogeography, Palaeoclimatology,
611 Palaeoecology 302, 243–254.
612 Eicher, D.L., 1969. Cenomanian and Turonian planktonic foraminifera from the Western Interior of
613 the United States. In: Fisher, D.L. (Ed.), Ist International Conference on Planktonic
614 Microfossils, Geneva, Switzerland, vol. 2. E.J. Brill, Leiden, pp. 163-174.
615 Eicher, D.L., Diner, R., 1985. Foraminifera as indicators of water mass in the Cretaceous Greenhorn
616 Sea, Western Interior. In: Pratt, L.M., Kauffman, E.G., Zelt, F.B. (Eds.), Fine-grained
617 deposits of cyclic sedimentary processes. SEPM Field Trip Guidebook, pp. 60–71.
618 Elderbak, K., Leckie, R.M., 2016. Paleocirculation and foraminiferal assemblages of the
619 Cenomanian-Turonian Bridge Creek Limestone bedding couplets: productivity vs. dilution
620 during OAE2. Cretaceous Research 60, 52-77.
621 Elderbak, K., Leckie, R.M., Tibert, N.E., 2014. Paleoenvironmental and paleoceanographic changes
622 across the Cenomanian-Turonian Boundary Event (Oceanic Anoxic Event 2) as indicated by
623 foraminiferal assemblages from the eastern margin of the Cretaceous Western Interior Sea.
624 Palaeogeography, Palaeoclimatology, Palaeoecology 413, 29–48.

625 Elder, W.P., 1987a. The Paleoecology of the CenomanianeTuronian (Cretaceous) stage boundary
626 extinctions at Black Mesa, Arizona. Palaios 2, 24–40.
627 Elder, W.P., 1987b. Cenomanian-Turonian (Cretaceous) stage boundary extinctions in the Western
628 Interior of the United States. Unpublished PhD thesis, University of Colorado, Boulder, 660
629 pp.
630 Elder, W.P., 1988. Geometry of Upper Cretaceous bentonite beds: implications about volcanic
631 source areas and paleowind patterns, Western Interior, United States. Geology 16, 835–838.
632 Elder, W.P., 1989. Molluscan extinction patterns across the Cenomaniane Turonian Stage boundary
633 in the Western Interior of the United States. Paleobiology 15, 299-320.
634 Elder, W.P., Kirkland, J.I., 1993. Cretaceous paleogeography of the Colorado plateau and adjacent
635 areas. Museum of northern Arizona Bulletin 59, 129-152.
636 Eldrett, J. S., Minisini, D., Bergman, S. C., 2014. Decoupling of the carbon cycle during Oceanic
637 Anoxic Event 2, Geology, 42, 567– 570, https://doi.org/10.1130/G35520.1, 2014.
638 Eldrett, J.S., Ma, C., Bergman, S.C., Lutz, B., Gregory, F.J., Dodsworth, P., Phipps, M., Hardas, P.,
639 Minisini, D., Ozkan, A., Ramezani, J., Bowring, S.A., Kamo, S.L., Ferguson, K., Macaulay,
640 C., Kelly, A.E., 2015. An astronomically calibrated stratigraphy of the Cenomanian, Turonian
641 and earliest Coniacian from the Cretaceous Western Interior Seaway, USA: Implications for
642 global chronostratigraphy. Cretaceous Research 56, 316–344.
643 Eldrett, J.S., Dodsworth, P., Bergman, C., Wright, M., Minisini, D., 2017. Water-mass evolution in
644 the Cretaceous Western Interior seaway of North America and equatorial Atlantic. Climate of
645 the Past 13, 855-878.
646 Fischer, C.G., Hay, W.W., Eicher, D.L., 1994. Oceanic front in the Greenhorn Sea (late middle
647 through late Cenomanian). Paleoceanography 9, 879-892.
648 Forster, A., Schouten, S., Moriya, K., Wilson, P.A., Sinninghe Damsté, J.S., 2007. Tropical
649 warming and intermittent cooling during the Cenomanian/Turonian oceanic anoxic event 2:
650 Sea surface temperature records from the equatorial Atlantic. Paleoceanography 22, PA1219,

651 doi: 10.1029/2006PA001349.
652 Fricke, H.C., Foreman, B.Z., Sewall, J.O., 2010. Integrated climate model-oxygen isotope evidence
653 for a North American monsoon during the Late Cretaceous. Earth and Planetary Science
654 Letters. 289, 11-21.
655 Gale, A.S., Christensen, W.K., 1996. Occurrence of the belemnite Actinocamax plenus in the
656 Cenomanian of SE France and its significance. Bulletin of the Geological Society of Denmark
657 43, 68–77.
658 Gertsch, B., Adatte, T., Keller, G., Tantawy, A.A.A.M., Berner, Z., Mort H.P., Fleitmann, D.,
659 2010a. Middle and late Cenomanian oceanic anoxic events in shallow and deeper shelf
660 environments of western Morocco. Sedimentology 57, 1430-1462.
661 Gertsch, B., Keller, G., Adatte, T., Berner, Z., Kassab, A.S., Tantawy, A.A.A., El-Sabbagh, A.M.,
662 Stueben, D., 2010b. Cenomanian-Turonian transition in shallow water sequence of the Sinai,
663 Egypt. International Journal of Earth Science 99, 165-182.
664 Glancy, T.J., Arthur, M.A., Barron, E.J., Kauffman, E.G., 1993. A paleoclimate model for the North
665 American Cretaceous (Cenomanian-Turonian) epicontinental sea, *in* Caldwell, W.G.E., and
666 Kauffman, E.G., eds., Evolution of the Western Interior basin: Geological Association of
667 Canada Special Paper 39, 219–241.
668 Grosheny, D., Beaudoin, B., Morel, L., Desmares, D., 2006. High-resolution biostratigraphy and
669 chemostratigraphy of the Cenomanian-Turonian event in the Vocontian Basin, southeast
670 France. Cretaceous Research 27, 629-640.
671 Hay, W.W., Eicher, D.L., Diner, R., 1993. Physical oceanography and water masses in the
672 Cretaceous Western Interior seaway. In: Caldwell, W.G.E., Kauffman, E.G. (Eds.), Evolution
673 of the Western Interior Basin. Geological Association of Canada Special Paper 39, 297–
674 318.
675 Haq, B.U., 2014. Cretaceous eustasy revisited. Global and Planetary Change 113, 44–58.
676 Hillier, S., Wilson, M.J., Merriman, R.J., 2006. Clay mineralogy of the Old Red Sandstone and

677 Devonian sedimentary rocks of Wales, Scotland and England. Clay Miner. 41, 433–471.
678 Huber, B.T., Norris, R., MacLeod, K.G., 2002. Deep-sea paleotemperature record of extreme
679 warmth during the Cretaceous. Geology 30, 123–126.
680 Jarvis, I., Gale, A.S., Jenkyns, H.C., Pearce, M.A., 2006. Secular variation in Late Cretaceous
681 carbon isotopes: a new $\delta^{13}C$ carbonate reference curve for the Cenomanian–Campanian
682 (99.6–70.6 Ma). Geological Magazine 143, 561–608.
683 Jarvis, I., Lignum, J.S., Gröcke, D.R., Jenkyns, H.C., and Pearce, M.A., 2011. Black shale
684 deposition, atmospheric CO2 drawdown, and cooling during the Cenomanian-Turonian
685 Oceanic Anoxic Event. Paleoceanography 26, PA3201.
686 Jenkyns, H.C., 2010. Geochemistry of oceanic anoxic events. Geochemistry, Geophysics,
687 Geosystems 11, Q03004, doi:10.1029/2009GC002788.
688 Jenkyns, H.C., Dickson, A.J., Ruhl, M., Van den Boorn, S.H.J.M., 2017. Basalt-seawater
689 interaction, the Plenus Cold Event, enhanced weathering and geochemical change:
690 deconstructing Oceanic Anoxic Event 2 (Cenomanian-Turonian, Late Creatceous).
691 Sedimentology 64, 16-43.
692 Joo, Y.J., Sageman, B.B., 2014. Cenomanian to Campanian carbon isotope chemostratigraphy from
693 the Western Interior Basin, U.S.A. Journal of Sedimentary Research 84, 529-542.
694 Jordan T.E., 1981. Thrust loads and foreland basin evolution, Cretaceous, western United States. -
695 American Association of Petroleum Geologists Bulletin, 65, 2506-2520.
696 Kauffman, E.G., 1977. Geological and biological overview: Western Interior Cretaceous Basin. The
697 Mountain Geologist 14, 75-99.
698 Kauffman, E.G., 1984. Paleobiogeography and evolutionary response dynamic in the Cretaceous
699 Western Interior Seaway of North America. In: Westermann, G.E.G. (Ed.), Jurassic-
700 Cretaceous biochronology and paleo- geography of North America. Geological Association of
701 Canada Special Paper 27, pp. 273–306.
702 Kauffman, E.G., 1985. Cretaceous evolution of the Western Interior Basin of the United States, in P

ratt, L.M., Kauffman, E.G. and Zelt, F.B., eds., Fine-Grained Deposits and Biofacies of the Cretaceous Western Interior Seaway: Evidence of Cyclic Sedimentary Processes: Society of Economic Paleontologists and Mineralogists, 1985 Midyear Meeting, Golden, Colorado, Field Trip Guidebook No. 4, p. iv-xiii.

Kauffman, E. G. and Caldwell, W G. E., 1993, The Western Interior Basin in space and time, in Caldwell, WG.E. and Kauffman, E.G., eds., Evolution of the Western Interior Basin: G eological Association of Canada, Special Paper 39, p. 1-30.

Keller, G., Berner, Z., Adatte, T., Stueben, D., 2004. Cenomanian–Turonian and 13C, and 18O, sea level and salinity variations at Pueblo, Colorado. Palaeogeogr. Palaeoclimatol. Palaeoecol. 211, 19–43.

Kennedy, W.J., Cobban, W.A., 1991. Stratigraphy and interregional correlation of the Cenomanian–Turonian transition in the Western Interior of the United States near Pueblo, Colorado, a potential boundary stratotype for the base of the Turonian Stage. Newsl. Stratigr. 24, 1–33.

Kennedy, W.J., Walaszczyk, I., Cobban, W.A., 2005. The global boundary stratotype section and point for the base of the Turonian stage of the cretaceous: Pueblo, Colorado, U.S.A. Episodes 28, 93–104.

Kirkland, J. I. 1991. Lithostratigraphic and biostratigraphic framework for the Mancos Shale (Late Cenomanian to Middle Turonian) at Black Mesa, northeastern Arizona; pp. 85-112 in J. D. Nations and J. G. Eaton (eds.), Stratigraphy, Depositional Environments, and Sedimentary Tectonics of the Western Margin, Cretaceous Western Interior Seaway, Geological Society of America Special Paper 260.

Kuhnt, W., Holbourn, A.E., Beil, S., Aquit, M., Krawczyk, T., Flögel, S., Chellai, E.L., Jabour, H., 2017. Unraveling the onset of Cretaceous Oceanic Anoxic Event 2 in an extended sediment archive from the Tarfaya-Laayoune Basin, Morocco. Paleoceanography 32, 923-946.

Kuypers, M.M.M., Pancost, R.D., Nijenhuis, I.A., Sinninghe Damsté, J.S., 2002. Enhanced productivity rather than enhanced preservation led to increased organic carbon burial in the

729 euxinic southern proto North Atlantic Ocean during the Cenomanian/Turonian Oceanic
730 Anoxic Event. Paleocenaography 17, 1051, doi:1029/2000PA000569.
731 Lanson, B., Meunier, A., 1995. La transformation des interstratifiés ordonnés (S ≥ 1) illite- smectite
732 en illite dans les série diagénétiques. État des connaissances et perspectives. Bull. Centre
733 Rech. Explor. Prod. Elf Aquitaine 19, 149–165.
734 Leckie, R.M., 1985. Foraminifera of the Cenomanian–Turonian Boundary Interval, Greenhorn
735 Formation, Rock Canyon Anticline, Pueblo, Colorado. In: Pratt, L.M., Kauffman, E.G., Zelt,
736 F.B. (Eds.), Fine-Grained Deposits Of Cyclic Sedimentary Processes. SEPM Field Trip
737 Guidebook, pp. 139–149.
738 Leckie, R.M., Schmidt, M.G., Finkelstein, D., Yuretich, R., 1991. Paleoceanographic and
739 paleoclimatic interpretations of the Mancos Shale (Upper Cretaceous), Black Mesa Basin,
740 Arizona, in Nations, J.D., and Eaton, J.G., eds., Stratigraphy, Depositional Environments, and
741 Sedimentary Tectonics of the western margin, Cretaceous Western Interior Seaway, Boulder,
742 Geological Society of America Special Paper 260p. 139-152.
743 Leckie, R.M., Yuretich, R.F., West, O.L.O., Finkelstein, D., Schmidt, M., 1998. Paleoceanography
744 of the southwestern Western Interior Sea during the time of the Cenomanian-Turonian
745 boundary (Late Cretaceous), in Stratigraphy and Paleoenvironments of the Cretaceous
746 Western Interior Seaway, USA, Concepts in Sedimentol. Paleontol., vol. 6, edited by W. E.
747 Dean and M. A. Arthur, pp. 101–126, Soc. Sediment. Geol., Tulsa, Okla.
748 Leckie, R. M., Bralower, T.J., Cashman, R., 2002. Oceanic anoxic events and plankton evolution:
749 Biotic response to tectonic forcing during the mid‐Cretaceous, Paleoceanography, 17(3),
750 1041, doi:10.1029/2001PA000623.
751 Ma, C., Meyers, S. R., Sageman, B. B., Singer, B. S., Jicha, B. R., 2014. Testing the astronomical
752 time scale for oceanic anoxic event 2, and its extension into Cenomanian strata of the Western
753 Interior Basin (USA). Geol. Soc. Am. Bull., doi:10.1130/b30922.1, 2014.
754 MacLeod, K.G., Martin, E.E., Blair, S.W., 2008. Nd isotopic excursion across Cretaceous ocean

anoxic event 2 (Cenomanian-Turonian) in the tropical North Atlantic. Geology 36, 811-814.

Martin, E.E., MacLeod, K.G., Jiménez Berrocoso, A., Bourbon, E., 2012. Water mass circulation on Demerara Rise during the Late Cretaceous based on Nd isotopes. Earth and Planetary Science Letters 327-328, 111–120.

Meyers, S., Siewert, S., Singer, B., Sageman, B., Condon, D., Obradovich, J., Jicha, B., Sawyer, D., 2012. Intercalibration of radioisotopic and astrochronologic time scales for the Cenomanian-Turonian boundary interval, Western Interior Basin, USA. Geology 40, 7-10.

Moore, D.M., Reynolds, R.C.J., 1997. X-Ray diffraction and the Identification and Analysis of Clay Minerals. Oxford University Press, New York, 378 pp.

Morel, L., 1998. Stratigraphie à Haute Résolution du passage Cénomanien-Turonien. Unpublished PhD Dissertation, Université Pierre et Marie Curie, Paris VI, 224pp.

Obradovich, J.D., Cobban, W.A., 1975. A time-scale for the Late Cretaceous of the Western Interior of North America, in Caldwell, W.G.E., ed., The Cretaceous system in the Western Interior of North America: Geological Association of Canada Special Paper. 13, 31-54.

O'Brien, C.L., Robinson, S.A., Pancost, R.D., Sinninghe Damsté, J.S., Schouten, S., Lunt, D.J., Alsenz, H., Bornemann, A., Bottini, C., Brassell, S.C., Farnsworth, A., Forster, A., Huber, B.T., Inglis, G.N., Jenkyns, H.C., Linnert, C., Littler, K., Markwick, P., McAnena, A., Mutterlose, J., Naafs, B.D.A., Püttmann, W., Sluijs, A., van Helmond, N.A.G.M., Vellekoop, J., Wagner, T., Wrobel, N.E., 2017. Cretaceous sea-surface temperature evolution: Constraints from TEX_{86} and planktonic foraminiferal oxygen isotopes. Earth-Science Reviews 172, 224-247.

Orth, C. J., Attrep, M.J., Quintana, L.R., Elder, W.P., Kauffman, E.G., Diner, R., Villamil T., 1993. Elemental abundance anomalies in the late Cenomanian extinction interval: A search for the source(s), Earth Planet. Sci. Lett., 117, 189–204.

Paul, C.R.C., Lamolda, M.A., Mitchell, S.F., Vaziri, M.R., Gorostidi, A., Marshall, J.D., 1999. The Cenomanian-Turonian boundary at Eastbourne (Sussex, UK): a proposed European reference

781 section. Palaeogeography, Palaeoclimatology, Palaeoecology 150, 83–121.
782 Petschick, R., 2000. MacDiff 4.2.5 manualAvailable at http://www.geologie.unifrankfurt.
783 de/Staff/Homepages/Petschick/PDFs/MacDiff_Manual_E.pdf 2000.
784 Pollastro, R.M., 1981. Authigenic kaolinite and associated pyrite in chalk of the Cretaceous
785 Niobrara Formation, eastern Colorado. Journal of Sedimentary Petrology 51, 553-562.
786 Poulsen, C.J., 1999, The mid-Cretaceous ocean circulation and its impact on greenhouse climate
787 dynamics [Ph.D. thesis]: University Park, Pennsylvania State University, 219 p.
788 Poulsen, C.J., Barron, E.J., Johnson, C.C., Fawcett, P.J., 1999. Links between the major climatic
789 factors and regional oceanography in the mid-Cretaceous. In: Barrera, E., Johnson, C.C.
790 (Eds.), Evolution of the Cretaceous ocean –climate system, pp. 73–90.
791 Poulsen, C.J., Pollard, D., White, T.S., 2007. GCM simulation of the δ18O content of continental
792 precipitation in the middle Cretaceous: a model-proxy comparison. Geology 35, 199-202.
793 Pratt, L.M., 1984. Influence of paleoenvironmental factors on preservation of organic matter in
794 middle Cretaceous Greenhorn Formation, Pueblo, Colorado. Am. Assoc. Pet. Geol. Bull. 68,
795 1146–1159.
796 Pratt, L.M., Threlkeld, C.N., 1984. Stratigraphic significance of $^{13}C/^{12}C$ ratios in mid-Cretaceous
797 rocks of the Western Interior, U.S.A. In: Stott, D.F., Glass, D.J. (Eds.), The Mesozoic of
798 Middle North America. Canadian Society of Petroleum Geologists, 9, pp. 305–312.
799 Pratt, L.M., Kauffman, E.G., Zelt, F.B. (Eds.), 1985. Fine-grained Deposits and Biofacies of the
800 Cretaceous Western Interior Seaway: Evidence of Cyclic Sedimentary Processes. Society of
801 Economic Paleontologists and Mineralogists, Tulsa.
802 Pratt, L.M., Arthur, M.A., Dean, W.E., Scholle, P.A., 1993. Paleo-oceanographic Cycles and Events
803 during the Late Cretaceous in the Western Interior Seaway of North America. In: Caldwell,
804 W.G.E., Kauffman, E.G. (Eds.), Evolution of the Western Interior Basin. Geol. Ass. Canada,
805 Spec. Pap., pp. 333–353.

R Core Team 2018. R: A language and environment for statistical computing. R Foundation for Statistical Computing, Vienna, Austria. URL https://www.R-project.org/.

Sageman B.B., 1996. Lowstand tempestites: depositional model for cretaceous skeletal limestones, Western Interior US. Geology 24, 888–892.

Sageman, B.B., Arthur, M.A., 1994. Early Turonian Paleogeographic/Paleobathymetric map, Western Interior, U.S. In: Caputo, M.V., Peterson, J.A., Franczyk, K.J. (Eds.), Mesozoic Systems of the Rocky Mountain Region, USA. SEPM, Rocky Mountain Section, pp. 457–470.

Sageman, B.B., Meyers, S.R., Arthur, M.A., 2006. Orbital time scale and new C-isotope record for Cenomanian-Turonian boundary stratotype. Geology 34, 125–128.

Schlanger, S.O., Jenkyns, H.C., 1976. Cretaceous oceanic anoxic events: Causes and consequences, Geol. Mijnbouw, 55, 179–184.

Schlanger, S. O., Arthur, M.A., Jenkyns, H.C., Scholle, P.A., 1987. The Cenomanian–Turonian oceanic anoxic event, I. Stratigraphy and distribution of organic carbon‐rich beds and the marine d13C excursion, in Marine Petroleum Source Rocks, edited by J. Brooks and A. J. Fleet. Geol. Soc. Spec. Publ. 26, 371–399.

Shaw, H.F., 2006. Clay mineralogy of Carboniferous sandstone reservoirs, onshore and offshore UK. Clay Miner. 41, 417–432.

Scaife, J.D., Ruhl, M., Dickson, A.J., Mather, T.A., Jenkyns, H.C., Percival, L.M.E., Hesselbo, P., Cartwright, J., Eldrett, J.S., Bergman, S.C., Minisini, D., 2017. Sedimentary mercury enrichments as a marker for submarine Large Igneous Province volcanism? Evidence from the Mid-Cenomanian Event and Oceanic Anoxic Event 2 (Late Cretaceous). Geochemistry, Geophysics, Geosystems. In press.

Sigal, J., 1977. Essai de zonation du Crétacé méditerranéen à l'aide des foraminifères planctoniques. Géologie Méditerranéenne 2, 99-108.

Singer, A., 1984. The palaeoclimatic interpretation of clay minerals in sediments – a review. Earth

Science Review 21, 251–293.

Sinninghe Damsté, J.S., van Bentum, E.C., Reichart, G.J., Pross, J., Schouten, S., 2010. A CO_2 decrease-driven cooling and increased latitudinal temperature gradient during the mid-Cretaceous Oceanic Anoxic Event 2. Earth and Planetary Science Letters 293, 97–103.

Skelton, P.W., Spicer, R.A., Kelley, S.P., Gilmour, I., 2003. The CretaceousWorld. Cambridge University Press, Cambridge.

Thiry, M., 2000. Palaeoclimatic interpretation of clay minerals in marine deposits: an outlook from the continental origin. Earth-Sci. Rev. 49, 201–221.

Tsikos, H., Karakitsios, V., van Breugel, Y., Walsworth-Bell, B., Bombardière, L., Petrizzo, M.R., Sinninghe Damsté, J.S., Schouten, S., Erba, E., Premoli Silva, I., Farrimond, P., Tyson, R.V., Jenkyns, H.C., 2004. Organic carbon deposition in the Cretaceous of the Ionian Basin, NW Greece: The Paquier event (OAE1b) revisited. Geological Magazine 141, 401–416.

Ufnar, D.F., Ludvigson, G.A., Gonzalez, L., Gröcke, D.R., 2008. Precipitations rates and atmospheric heat transport during the Cenomanian greenhouse warming in North America: Estimates from a stable isotope mass-balance model. Palaeogeography, Palaeoclimatology, Palaeoecology 266, 28-38.

van Helmond, N.A.G.M., Sluijs, A., Reichart, G.J., Sinninghe Damsté, J.S., Slomp, C.P., 2014. A perturbed hydrological cycle during Oceanic Anoxic Event 2. Geology 42, 123–126.

Weimer R.J., 1984. Relationship of Unconformities, Tectonics, and Sea Level Changes in the Cretaceous of the Western Interior, United States. In: SCHLEE J. S., ed. Interregional unconformities and hydrocarbon accumulation. - AAPG memoir, 36, 7-35.

White, T., Gonzalez, L., Ludvigson, G., Poulsen, C., 2001. Middle Cretaceous greenhouse hydrologic cycle of North America. Geology 29, 63-66.

Yule, G. U. 1926. 'Why do we sometimes get nonsense-correlations between Time-Series?--a study in sampling and the nature of time-series', Journal of the royal statistical society, Vol. 89, pp. 1-63.

858

859 **Figure captions**

860

861 **Fig. 1:** Palaeoceanographic map of the Western Interior Basin showing the circulation pattern in the
862 basin with the incursion of southern Tethyan water masses and possible local source of clay
863 minerals (modified from Leckie et al., 1998). Metal abundance anomalies have been reported
864 according to the study of Orth et al. (1993).

865

866 **Fig. 2:** Distribution of the percentage of sinistral *M. delrioensis*, and $\delta^{18}O_{carb}$ records (Desmares et
867 al., 2016) compared with the changes in the clay mineral assemblage in the Cenomanian-Turonian
868 interval of Pueblo (Colorado).

869

870 **Fig. 3:** Distribution of the percentage of sinistral *M. delrioensis*, and $\delta^{18}O_{carb}$ records (Desmares et
871 al., 2016) compared with the changes in the clay mineral assemblage in the Cenomanian-Turonian
872 interval of Hot Springs (South Dakota).

873

874 **Fig. 4:** Distribution of the changes in the clay mineral assemblages in the Cenomanian-Turonian
875 interval of Lohali Point (Arizona) and Elm (Kansas).

876

877 **Fig. 5:** Scanning electron microscope examinations of the internal content of foraminiferal test at
878 Hot Springs, A) and B) HS3 (*S. gracile* ammonite zone, kaolinite content: 36%), C) and D) HS5 (*S.*
879 *gracile* ammonite zone, kaolinite content: 46%), E) and F) HS9 (*S. gracile* ammonite zone,
880 kaolinite content: 32%), G) and H) HS26 (*N. juddii* ammonite zone, kaolinite content: 7%), I) and J)
881 HS62 (*P. flexuosum* ammonite zone, kaolinite content: 29%).

882

883 **Fig. 6:** Distribution of kaolinite and R0 I-S contents compared with the changes in the percentage of

884 sinistral *M. delrioensis* and $\delta^{18}O_{carb}$ records in the section at Pueblo and Hot Springs (Desmares et
885 al., 2016). The age model, in regard to the beginning of the marker bed 63, is based on the
886 cyclostratigraphic approach of Sageman et al. (2006) and Meyers et al. (2012). The stratigraphic
887 framework is given by ammonite biozonation (Leckie, 1985; Kennedy and Cobban, 1991) and by
888 the position of the bentonite marker beds A, B, C, and D. The blue dashed lines indicate the periods
889 that are described in the discussion.
890
891 **Table 1:** Correlations between kaolinite and environmental variables ($\delta^{18}O_{carb}$ and % sinistral form
892 of *M. delrioensis*) for Hot Springs sections. Short and long term relationships are investigated
893 thanks to non-overlapping moving average. Window corresponds to the number of values taken to
894 calculate each average. Cor: Pearson correlation coefficient; pvalue: pvalue of cor.test using
895 Pearson correlation; I: number of times differences have been computed to remove autocorrelation;
896 n: number of values used for each correlation. Pvalues under 0.1 are highlighted in bold.

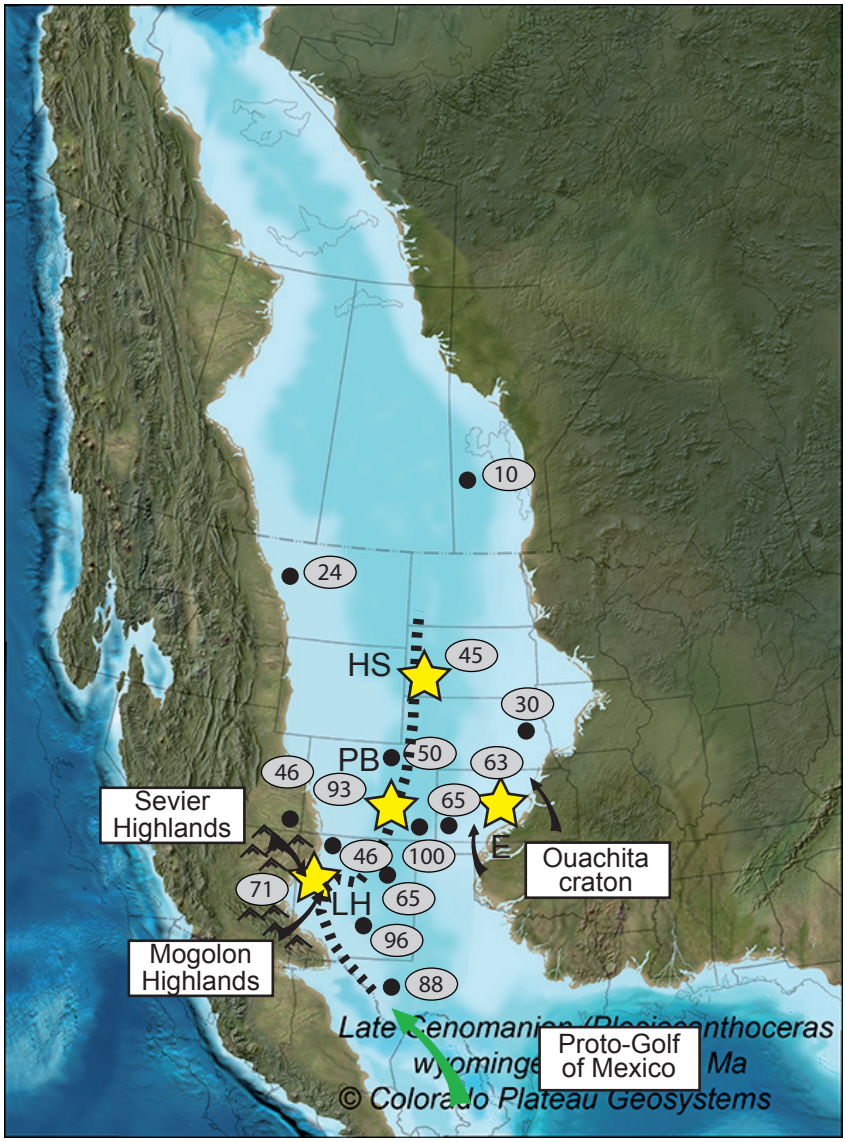

Legend:

- circulation pattern
- Tethyan waters
- 100 — Metal abundance anomalies (greatest deposition assigned a value of 100)
- Possible local source of clay minerals
- Sections studied in this study
  - HS: Hot Springs
  - E: Elm
  - PB: Pueblo
  - LH: Lohali Point

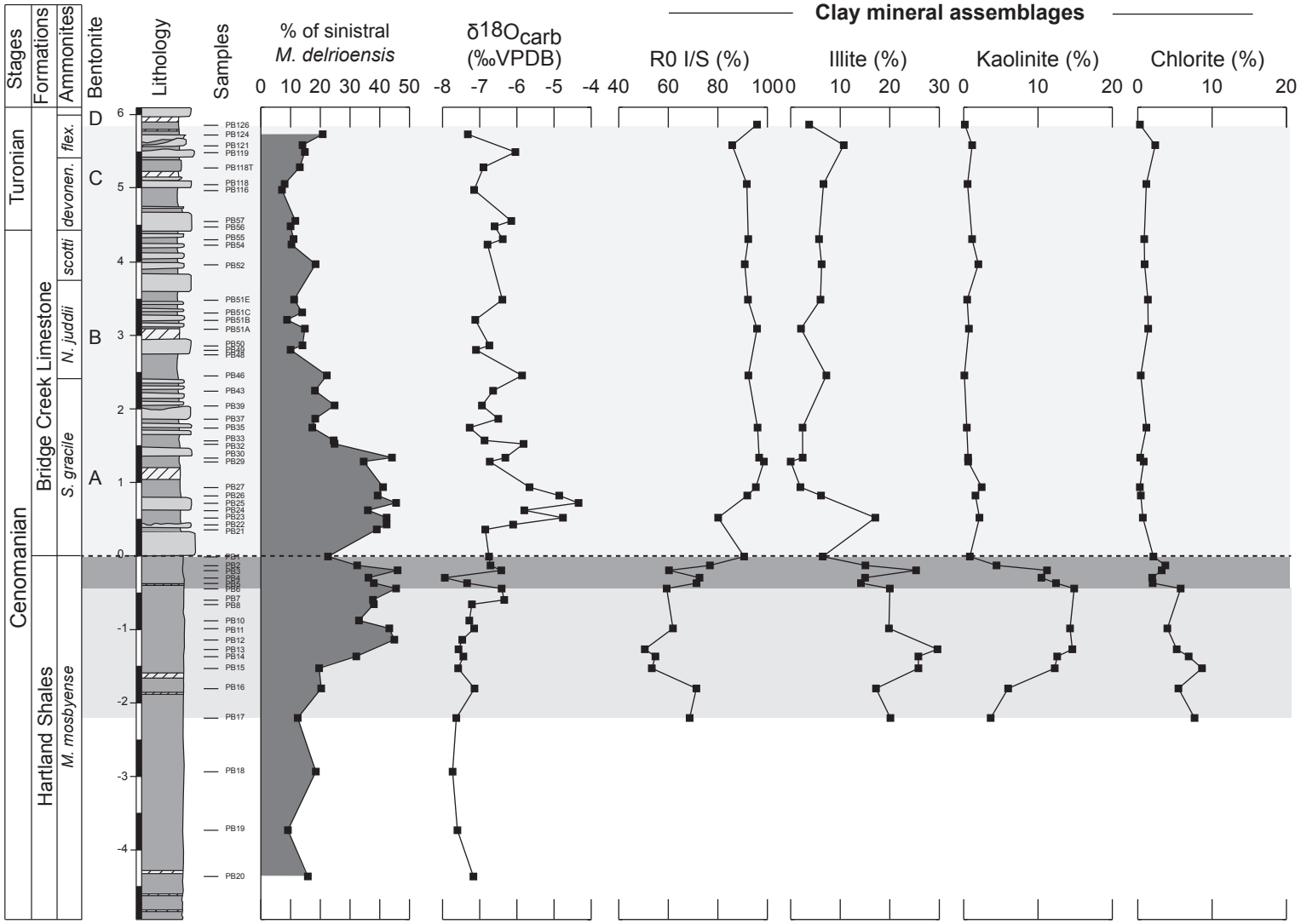
Pueblo (Colorado)
Stages
Formations
Ammonites
Bentonite
Lithology
Samples
% of sinistral
M. delrioensis
δ18Ocarb
(‰VPDB)
Clay mineral assemblages
R0 I/S (%)
Illite (%)
Kaolinite (%)
Chlorite (%)
Turonian
Cenomanian
Bridge Creek Limestone
Hartland Shales
flex.
devonen.
scotti
N. juddii
S. gracile
M. mosbyense
D
C
B
A
(Desmares et al., 2016)

Hot Springs (South Dakota)

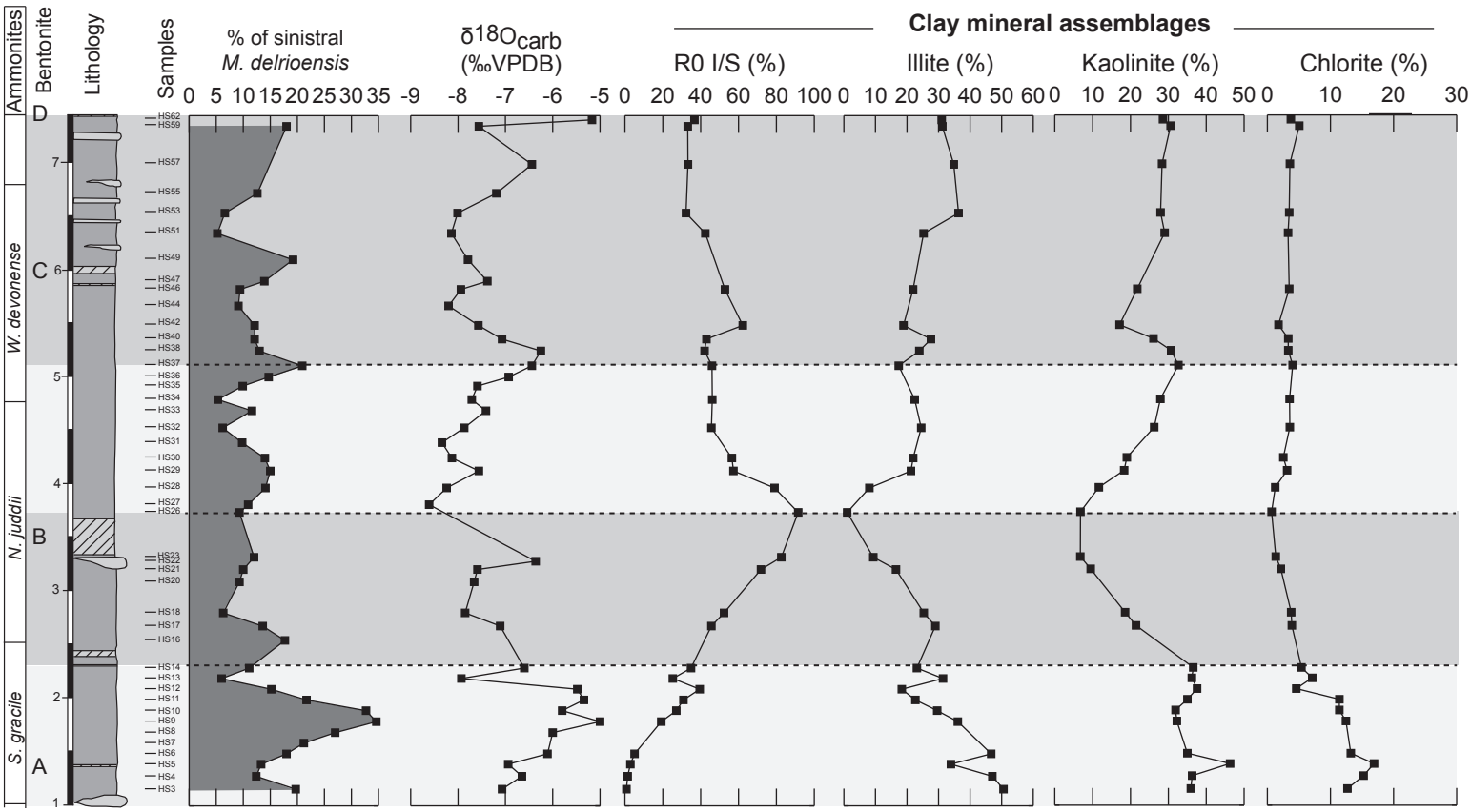

(Desmares et al., 2016)

western and eastern marginal sections

Lohali Point (Arizona)

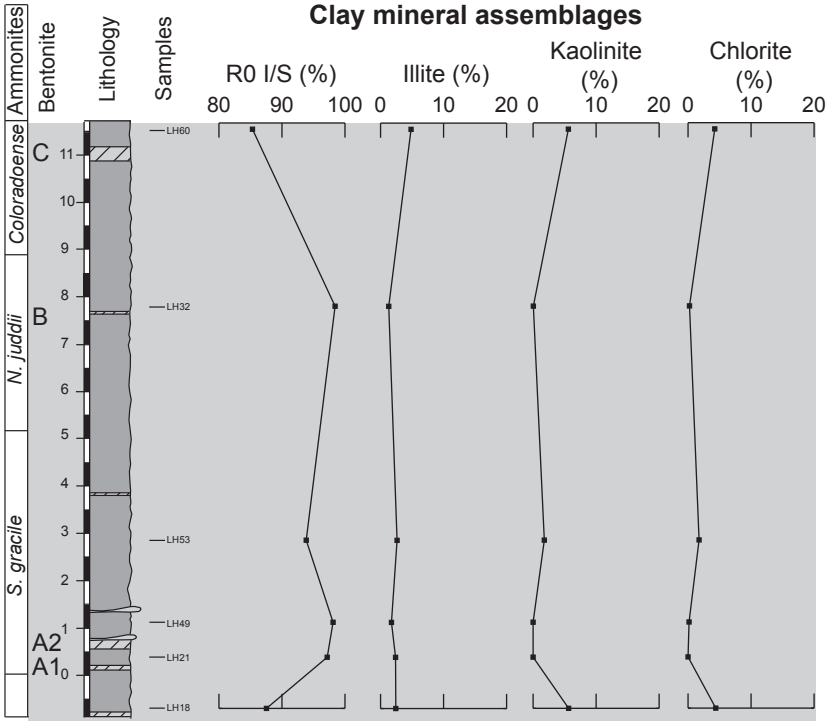

Elm (Kansas)

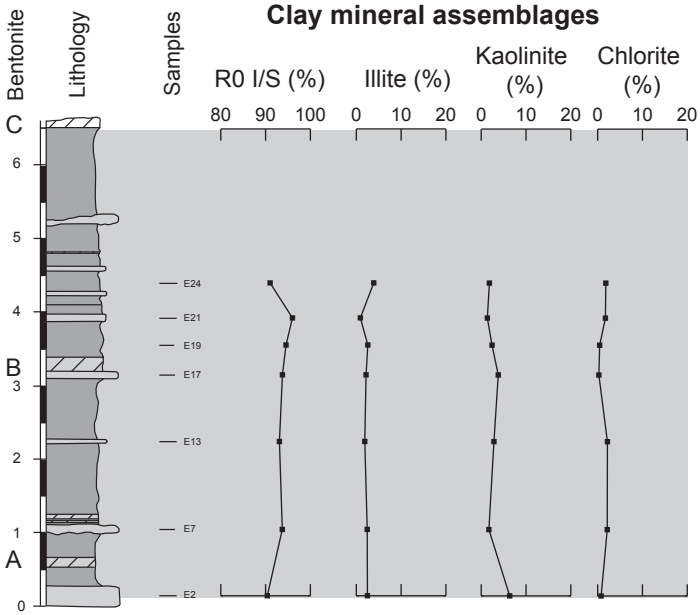

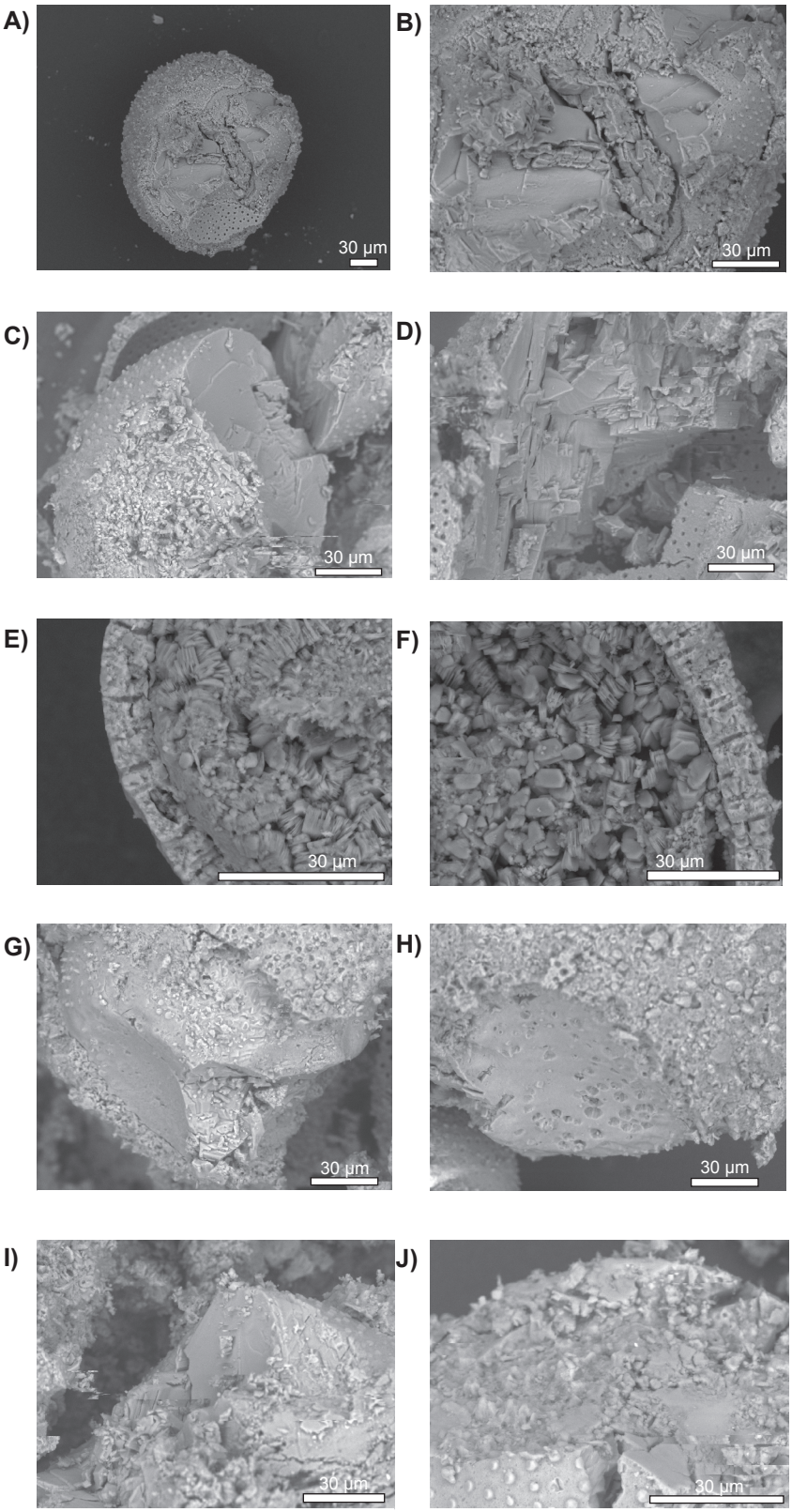
A)
30 µm
B)
30 µm
C)
30 µm
D)
30 µm
E)
30 µm
F)
30 µm
G)
30 µm
H)
30 µm
I)
30 µm
J)
30 µm

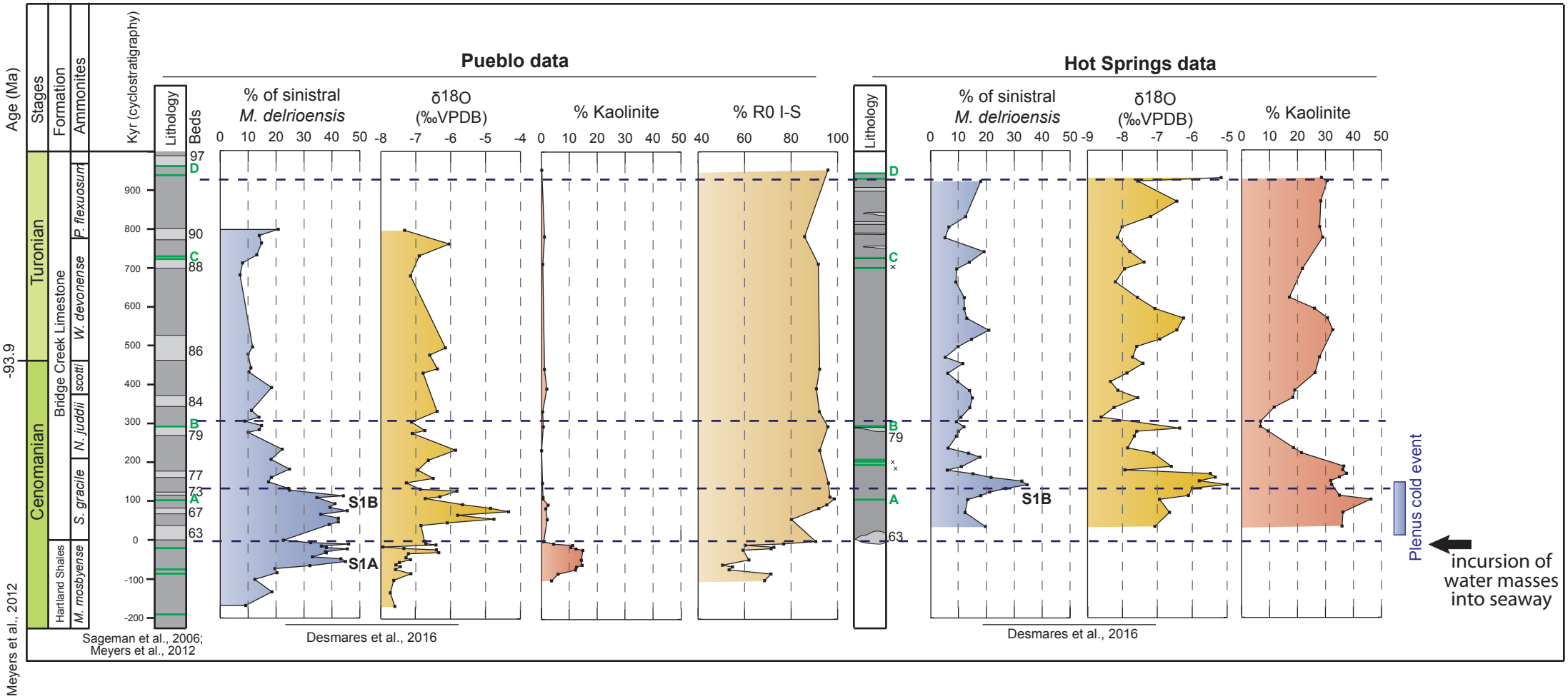
Age (Ma)
Stages
Formation
Ammonites
Kyr (cyclostratigraphy)
Lithology
Beds
Pueblo data
% of sinistral M. delrioensis
δ18O (‰VPDB)
% Kaolinite
% R0 I-S
Hot Springs data
Turonian
Cenomanian
Bridge Creek Limestone
Hartland Shales
P. flexuosum
W. devonense
scotti
N. juddii
S. gracile
M. mosbyense
-93.9
D
C
B
A
S1B
S1A
Plenus cold event
incursion of water masses into seaway
Sageman et al., 2006; Meyers et al., 2012
Desmares et al., 2016
Meyers et al., 2012

		Hot Spring							
		δ18O				sinistral			
	Window	cor	pvalue	I	n	cor	pvalue	I	n
kaolinite	1	0.05	0.82	1	27	-0.13	0.53	1	27
	2	0.21	0.50	1	13	-0.23	0.45	1	13
	3	**0.71**	**0.03**	**0**	**9**	0.37	0.33	0	9
	4	**0.74**	**0.06**	**0**	**7**	0.49	0.26	0	7
	5	**0.91**	**0.03**	**0**	**5**	**0.96**	**0.01**	**0**	**5**